Research article

Carbon Future

Engineered interface in sunlight-driven non-oxidative ethane dehydrogenation

Zexuan Li[1,2], Chenwei Ni[1], Ping Jin[1,2]✉, Yu Wang[3], Feng Wang[1,2,4]✉

[1] *State Key Laboratory of Catalysis, Dalian National Laboratory for Clean Energy, Dalian Institute of Chemical Physics, Chinese Academy of Sciences, Dalian 116023, China.*

[2] *University of Chinese Academy of Sciences, Beijing 100049, China.*

[3] *Shanghai Synchrotron Radiation Facility, Shanghai Advanced Research Institute, Chinese Academy of Sciences, Shanghai 201204, China.*

[4] *New Cornerstone Science Laboratory, Dalian·116023, China.*

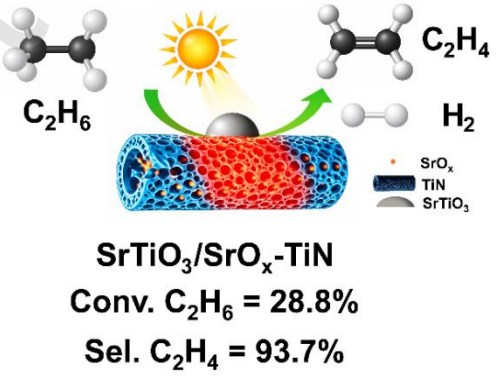
Carbon Future 2026, 3, 9200093 https://doi.org/10.26599/CF.2026.9200093

Received: July 29, 2026; **Revised:** October 9, 2026; **Accepted:** November 2, 2026

✉Address correspondence to Ping Jin, pingjin@dicp.ac.cn; Feng Wang, wangfeng@dicp.ac.cn.

ORCID ID of the corresponding author: Ping Jin, 0000-0001-8741-7738; Feng Wang, 0000-0002-9167-8743.

ABSTRACT: Photocatalytic reactions powered by solar energy are essential for capitalizing on renewable solar resources. However, efficiently utilizing the entire sunlight spectrum for reactions with high activation energy, such as alkane dehydrogenation, poses a major challenge in catalyst design. In this research, we propose a surface modification strategy that generates abundant interfacial sites on the TiN surface while preserving strong light absorption, promoting interfacial electron-hole recombination, and supporting catalytic reactions across the full spectrum. Through a combination of spectroscopic, theoretical, and experimental investigations, we demonstrate the effectiveness of this catalyst design in enhancing solar energy utilization. We have successfully developed a $SrTiO_3/SrO_x$-TiN catalyst that significantly enhances the activity of non-oxidative ethane dehydrogenation by 11.7-fold under solar photocatalysis. The strategy revealed in this work, which involves constructing abundant reaction sites with enhanced interfacial electron-hole recombination, is vital for developing advanced heterogeneous solar photocatalytic systems.



KEYWORDS: Surface modification, titanium nitride, sunlight-driven, ethane dehydrogenation.

1 Introduction

Solar energy is the most abundant renewable energy resource on Earth[1]. Effectively harnessing it to drive chemical transformations and produce high-value chemicals is of considerable importance[2,3,4]. Among solar energy conversion pathways, solar thermal catalysis stands out by converting solar energy into thermal energy on catalyst surfaces, generating localized high-temperature hot spots on the catalyst surface[5]. These surface sites efficiently promote chemical transformations, enabling the conversion of solar energy into chemical energy and making solar thermal catalysis a promising approach for high-efficiency solar energy utilization. Achieving efficient solar thermal catalysis requires not only chemically stable, reaction-specific catalytic sites[6] to direct the selective conversion of reactant molecules and intermediates, but also the rational regulation of catalyst electronic structure[7] and geometric morphology[8,9] to optimize solar spectrum absorption and photothermal conversion efficiency, both of which are essential for maximizing solar-to-chemical energy conversion. Existing systems used surface-loaded metals[10] to influence the interaction between the metal and the support, which modifies the interfacial geometric or electronic structure and promotes the reaction when exposed to light of a specific or relatively narrow wavelength[11, 12]. Transition metal nitrides, such as titanium nitride, have garnered significant attention in solar thermal catalysis, particularly for photothermal CO_2 hydrogenation[13] and photothermal biomass oxidation[14], due to their broad localized surface plasmon resonance (LSPR)-induced absorption across the solar spectrum and the abundance of surface sites[15]. This indicates that the LSPR of this TiN with a proportion of Au, etc., has a wider absorption range and higher absorption efficiency. Nevertheless, transition metal nitrides typically possess a limited number of surface active sites and exhibit relatively low solar-to-chemical energy conversion efficiency[16]. Additionally, the characteristics of oxygen species present on the nitride surface play a critical role in determining catalytic performance, with interfacial regions frequently serving as highly active reaction sites[17]. Furthermore, during photothermal reduction or oxidation, over-oxidation or nitrogen loss occurs[13,14], which further reduces the photo-to-thermal conversion efficiency of nitrides[18,19]. Consequently, developing nitride catalysts that combine an abundance of highly active sites with robust and efficient photothermal conversion under high-temperature and reductive atmosphere conditions remains a significant challenge.

To address this challenge, we propose modifying TiN with alkaline earth metal ions (Sr, Ca, Mg, La, Ce , Sm and Ba) to generate high-dielectric-constant, irreducible $MTiO_3$–TiN interface species, with the objective of red-shifting LSPR absorption band[20] and thereby enhancing photothermal efficiency[21]. Meanwhile, incorporating electron-withdrawing

Just Accepted

$MTiO_3$ (such as $SrTiO_3$) species facilitates electron extraction from the electron-rich TiN substrate, lowering the overall work function of the TiN material[22] and enhancing interfacial electron-hole recombination. This process generates localized high temperatures directly at the interface sites, making it more efficient than thermalcatalysis. In photothermal non-oxidative ethane dehydrogenation (NOEDH), Sr-modified TiN exhibited a 11.7-fold enhancement in ethylene formation rate compared to unmodified TiN, with ethylene selectivity reaching up to 94%. This represents the first reported nitride-based catalyst with high olefin selectivity for NOEDH, outperforming almost all previously reported photothermal NOEDH catalysts (Table. S1)[11,23,24,25-27]. Reaction results and cycling experiments confirmed that the modified $SrTiO_3/SrO_x$-TiN catalyst exhibits excellent activity and stability for ethane dehydrogenation. Furthermore, over four consecutive days under natural sunlight, we showed that the catalyst can reach a maximum ethylene production rate of 1846 μmol h^{-1} with 85.9% selectivity. Overall, this work provides an effective modification strategy and valuable guidance for the design of nitride catalysts for NOEDH, combining robust stability with high photothermal conversion efficiency.

2 Results and discussion

2.1 Structure of $SrTiO_3/SrO_x$-TiN nanocomposite.

The TiN catalyst (Fig. 1a) was synthesized using $H_2Ti_4O_9$ nanotubes as the titanium source. Metal precursors were impregnated onto the nanotube surfaces, then nitrided by ammonia calcination at a temperature between the N-doping temperature of TiO_2 ($T_{N,TiO2}$) and that of $MTiO_3$ ($T_{N,MTiO3}$). The Sr-modified catalyst serves as a representative example. For comparison, an unmodified catalyst was prepared under identical conditions without metal precursors.

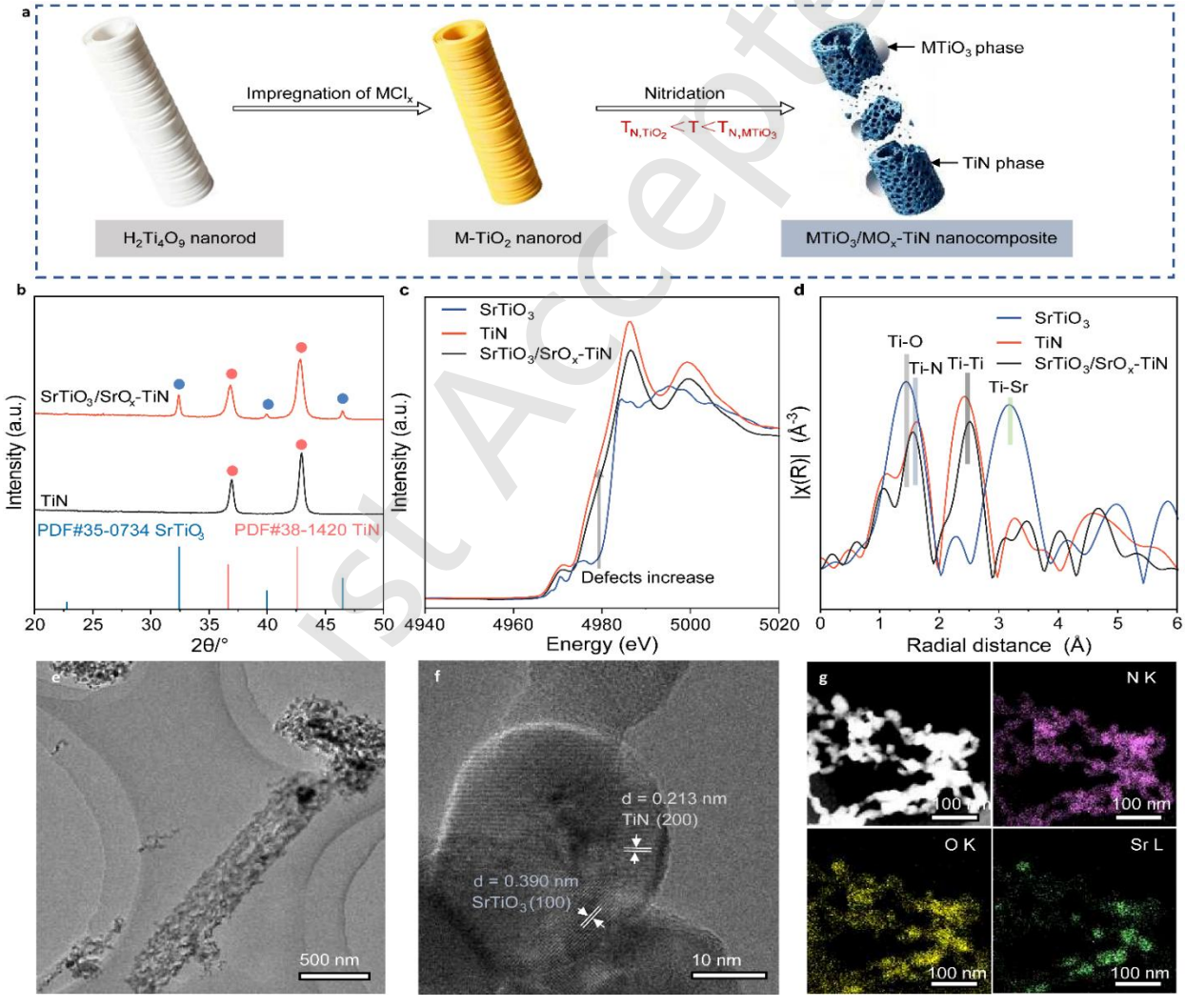


Fig. 1. Preparation of photothermal catalyst $SrTiO_3/SrO_x$-TiN. (**a**) Schematic diagram of catalyst preparation. (**b**) The X-ray diffraction (XRD) patterns of TiN and $SrTiO_3/SrO_x$-TiN catalysts. HRTEM image of $SrTiO_3/SrO_x$-TiN. (**c**) X-ray absorption near edge structure (XANES) of TiN before and after $SrTiO_3$ modification. (**d**) Ti K-edge XAFS spectra of TiN before and after Sr modification. (**e**) The HRTEM image of $SrTiO_3/SrO_x$-TiN. (**f**) The HRTEM image of the interface of $SrTiO_3/SrO_x$-TiN. (**g**) HAADF-STEM image of $SrTiO_3/SrO_x$-TiN and energy-dispersive X-ray spectroscopy (EDS) mappings showed the spatial distribution of N K, O K, and Sr L edge.

1st Accepted

XRD patterns show two sets of diffraction peaks (Fig. 1b) corresponding to TiN and $SrTiO_3$ crystalline phases, likely resulting from a high-temperature reaction between $SrCl_2$ and TiO_2 formed during dehydration. $SrCl_2$ was not found to change the morphology of the nanotube (Fig. S1). Compared to pure TiN, the (200) reflections of TiN in the nanocomposite shift to higher angles, indicating lattice contraction. XANES analysis places the Sr-modified catalyst between TiN and $SrTiO_3$, suggesting a lower defect concentration than in the unmodified sample. The Ti K-edge XAFS spectra confirm a corresponding shift in Ti–N bond lengths[12,28] (Fig. 1d). HRTEM images reveal a nitrided structure of partially fractured nanotubes (Fig. 1e), composed of strongly agglomerated particles 20 to 40 nm in diameter (Fig. 1f). HRTEM analysis shows lattice fringes for the (200) plane of TiN and the (110) plane of $SrTiO_3$, confirming the nanotubes consist of both $SrTiO_3$ and TiN particles. For unmodified TiN (Figs. 1b and S2c), the main exposed planes are (200) and (111); comparison of the TiN (200) lattice spacing before and after modification further confirms the lattice contraction.

EDS analysis of the TiN regions (Fig. 1g) shows a uniform distribution of O and Sr. Since the atomic radius of Sr^{2+} is larger than that of Ti^{3+}, Sr incorporation into the TiN lattice would be expected to cause lattice expansion and shift the TiN XRD peaks to lower angles. However, this is not observed experimentally (Fig. 1b). Therefore, Sr is concluded to be present mainly as an $SrTiO_3$ phase on the TiN surface.

2.2 Enhanced photo-to-thermal conversion.

To evaluate photo-to-thermal conversion efficiency before and after Sr modification, we systematically examined light absorption and carrier recombination in both nanocomposites and pristine TiN.

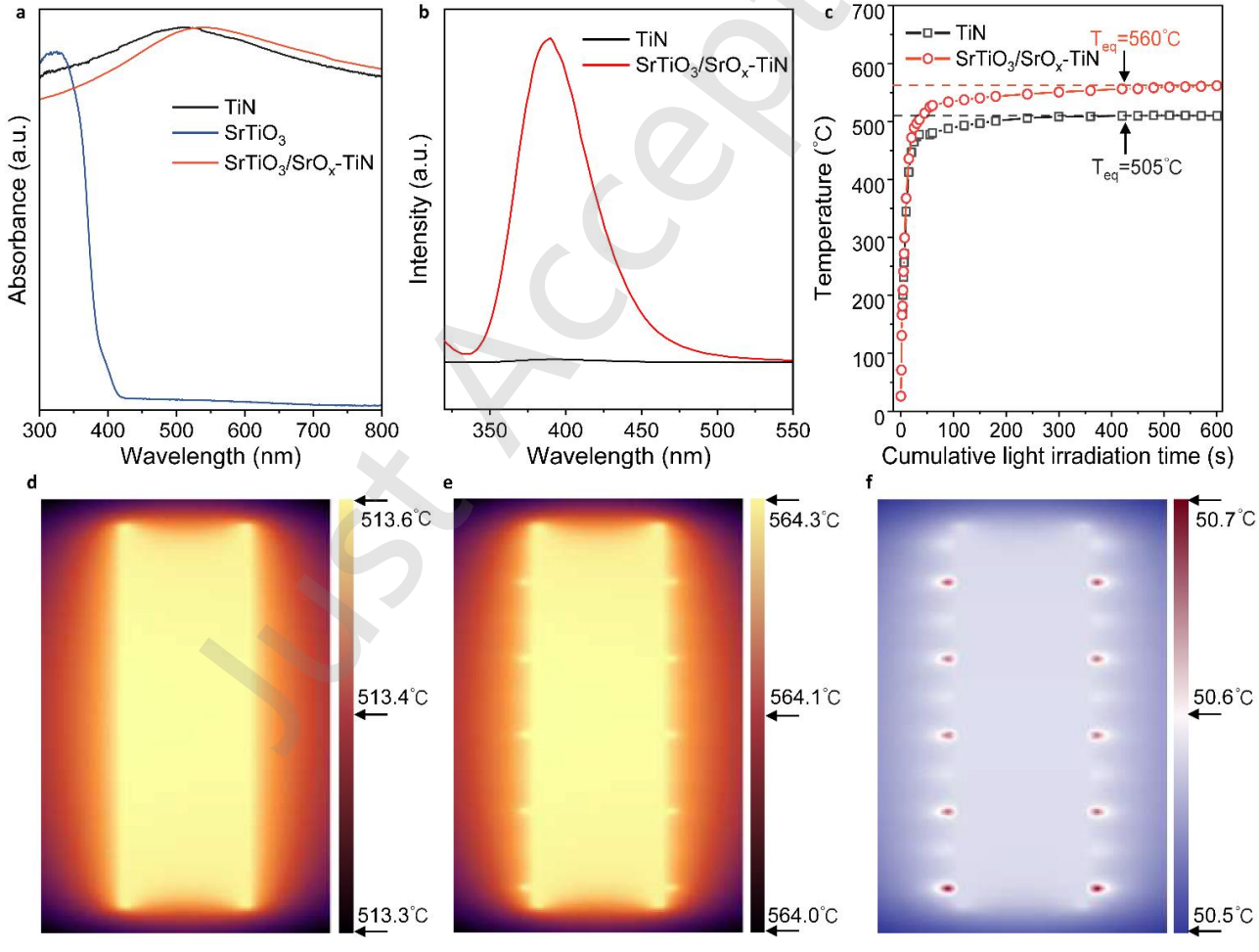


Fig. 2. Investigation of the photothermal mechanism before and after $SrTiO_3$ modification. (**a**) UV-vis absorption spectra of the catalysts. (**b**) The Photoluminescence Spectroscopy (PL) patterns of TiN and $SrTiO_3/SrO_x$-TiN catalysts. (**c**) Temperature profiles of TiN (black dot-line) and $SrTiO_3/SrO_x$-TiN (red dot-line). To test light-to-heat conversion efficiency, 60 mg catalyst was compressed into the metallic round groove, and the gas atmosphere was changed to 1 atm Ar. Then the Xenon lamp was turned on with 7.74 W cm^{-2} irradiation, and the real-time temperature profile was recorded. The equilibrium temperature was taken as the temperature at which the temperature fluctuation was relatively small. COMSOL simulation of the surface temperature of (**d**) TiN and (**e**) $SrTiO_3/SrO_x$-TiN after focusing sunlight. (**f**) Temperature change on the catalyst surface after $SrTiO_3$ modification for the $SrTiO_3/SrO_x$-TiN.

Just Accepted

UV-Vis diffuse reflectance spectra show a slight increase in low-energy photon utilization for $SrTiO_3/SrO_x$-TiN nanocomposites (Fig. 2a). The transverse-mode LSPR peak of TiN in the nanocomposites shifts from 517 nm to 538 nm, indicating improved visible-light harvesting. Photoluminescence spectra (Fig. 2b) confirm that the nanocomposites have better carrier recombination properties than pure TiN. These results demonstrate significant differences in solar light absorption and utilization between Sr-modified and unmodified TiN catalysts.

Solar-to-thermal conversion experiments were conducted using a metal reactor with a quartz window (Figs. S4 and S5), measuring the near-surface temperatures of pure TiN and $SrTiO_3/SrO_x$-TiN nanocomposite. Under illumination, the Sr-modified TiN reached a steady-state surface temperature 55 °C higher than the unmodified sample (Fig. 2c), indicating improved photo-to-thermal conversion efficiency. Through Differential Scanning Calorimetry (DSC) and photo-to-thermal measurements, we analyze the photothermal conversion efficiencies of TiN and $SrTiO_3/SrO_x$-TiN. The results showed that Sr modification improved the interfacial light-to-heat efficiency by approximately 18% (Fig. S6). COMSOL simulations modeled surface temperature distributions before and after modification (Figs. 2d–2f). Without illumination, catalyst surface temperatures remained unchanged (Fig. 2c and Fig. S7a). When interfacial electron-hole recombination was allowed (Fig. S7b), the modified catalyst's surface temperature increased with recombination power; at 9×10^{-9} W, the TiN surface temperature reached about 564 °C (Fig. 2e). The simulated temperature increase of 51 °C closely matches the experimental difference of 55 °C. These results confirm that electron-hole recombination at the TiN/$SrTiO_3$ interface drives the enhanced photothermal effect. Overall, metal-ion modification significantly improves the solar-to-thermal conversion efficiency of TiN, supporting further study of its use in solar-driven thermalcatalytic C–H bond activation.

2.3 Photothermal non-oxidative ethane dehydrogenation.

We evaluated the catalytic performance of TiN catalysts for NOEDH before and after surface modification.

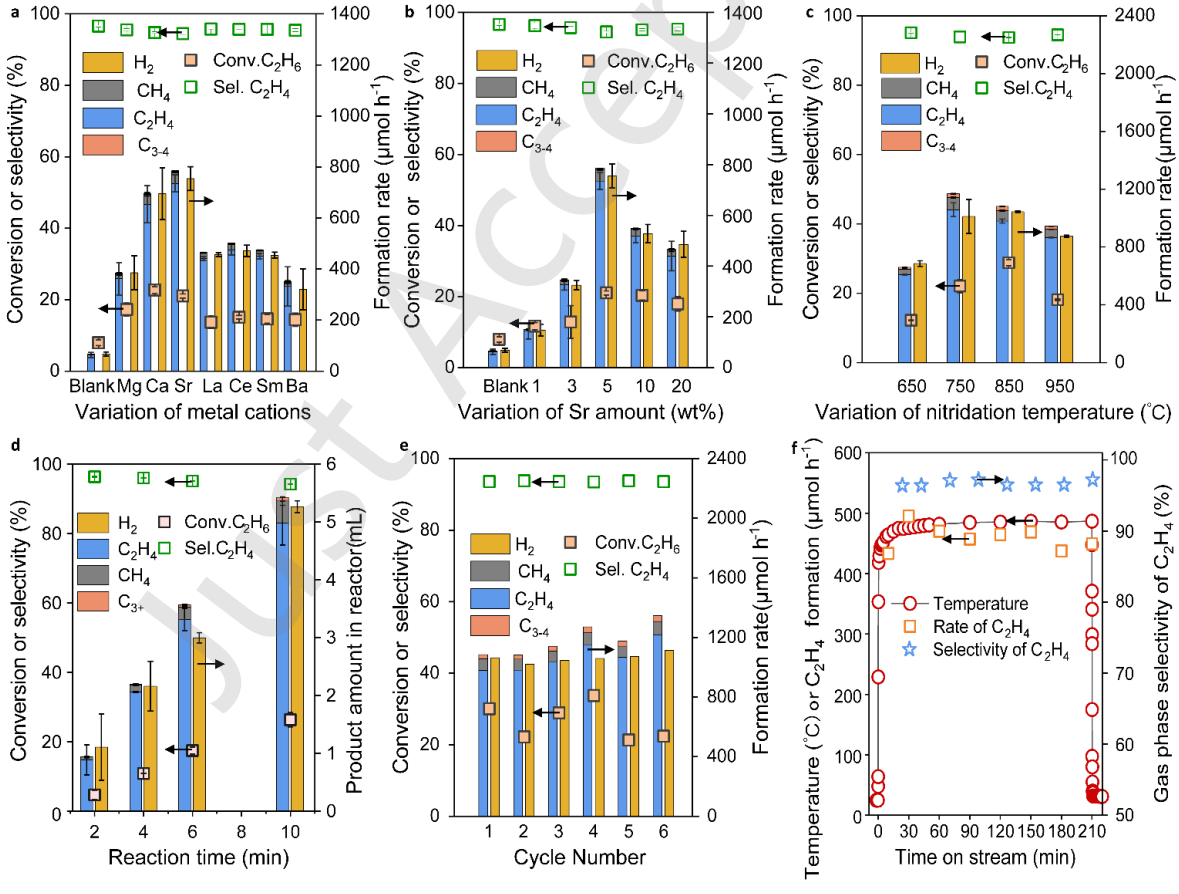


Fig. 3. Effect of different modified catalysts on photocatalytic non-oxidative ethane dehydrogenation. (**a**) Catalysts with different cation loadings. (**b**) Catalysts with different Sr loadings. (**c**) Catalysts with different nitridation temperatures. (**d**) Reaction time profile of photothermal ethane dehydrogenation. (**e**) Ethane dehydrogenation cycle reaction. (**f**) Photothermal ethane dehydrogenation in flow reaction. Batch reaction conditions: 20 mL C_2H_6 was injected into a 40 mL metallic reactor filled with 1 atm Ar, and 60 mg catalyst was compressed into the metallic round groove and irradiated by 7.74 or 10.4 W cm^{-2} full-spectrum xenon light for 10 minutes. Flow reaction conditions: 1 atm, 25 mL $minute^{-1}$ 19.9% C_2H_6/N_2, 60 mg catalyst, 7.74 W cm^{-2} simulated solar irradiation, every 30 minutes gas components were extracted for analysis. Data in Figure 3a and 3b are repeated three times and two times for data in other figures.

Just Accepted

The unmodified TiN catalyst showed an ethylene (C_2H_4) formation rate of 62.6 μmol h^{-1} and a selectivity of 96.6%. Incorporating alkaline-earth metal ions consistently enhanced activity; the Sr-modified catalyst showed the greatest improvement, with a C_2H_4 formation rate of 735 μmol h^{-1} (a 11.7-fold increase) and a selectivity of 94.5%. The hydrogen production energy efficiency was determined to be 20.82 μmol H_2 kJ^{-1} based on H_2 production amount and light intensity. The Ca-modified catalyst showed similar enhancement, followed by Mg-, La-, Ce-, Sm- and Ba-modified catalysts. XRD patterns indicated distinct perovskite phases in Ca-, La-, Ce-, Sm-, and Sr-containing samples, while no oxide crystal peaks were observed in Mg- or Ba-containing samples (Fig. S8).

To identify the catalyst's active sites, we conducted control experiments using a TiN/$SrTiO_3$ physical mixture with the same phase ratio as $SrTiO_3$/SrO_x-TiN, and a catalyst with 10 wt% $SrTiO_3$ prepared by the same method (Fig. S9). Both showed catalytic performance similar to pure TiN, indicating $SrTiO_3$ alone is not active. Thus, the TiN/$SrTiO_3$ interface was likely the main active site. The interfacial reaction temperature was measured with thermocouples and an infrared camera (Fig. S10), showing an approximately 50 °C increase after Sr modification, consistent with COMSOL simulation results. To distinguish the thermalcatalytic mechanism, NOEDH was carried out at various temperatures. The findings (Fig. S11) indicated that Sr modification negatively affected NOEDH across the entire heating range. It is hypothesized that the active thermalcatalytic site resides on TiN, and the Sr surface modification, which covers the TiN surface, hampers the reaction. Sr loading experiments further support this: as Sr content increased from 1 wt% to 20 wt%, activity peaked at 5 wt% and then declined, due to optimal exposure of interfacial sites at 5 wt% and subsequent coverage by $SrTiO_3$ at higher loadings, as shown by XRD (Fig. S12). Adjusting calcination temperature (Fig. S13) showed that 850 °C produced the best catalytic activity and stability (Figs. 3c, S14, and S15).

To evaluate SrO_x stability in the nanocomposite, we adjusted the spotlight radius (Fig. S4b) and increased light intensities (Fig. S16). Monitoring H_2 and C_2H_4 yields during illumination (Fig. 3d) showed the H_2/C_2H_4 ratio remained close to the theoretical 1:1. Cycling experiments (Fig. 3e) confirmed no significant catalyst deactivation, even at higher light intensities and temperatures, with the ethylene-to-hydrogen production ratio consistently near 1:1. These results demonstrate the strong stability of SrO_x on the TiN surface.

Post-reaction XRD (Fig. S17b) showed no significant changes compared to the fresh catalyst, confirming the stability of both TiN and surface SrO_x. The structure of the catalyst after the reaction was characterized by HRTEM and EDS mapping (Fig. S18), and the results showed that the structure did not change significantly before and after the reaction. Further XPS spectroscopy also indicated partial surface N and O consumption on the catalyst surface before and after the reaction (Fig, S19). EPR analysis further confirmed that there were negligible O or N vacancies during C_2H_6 dehydrogenation (Fig. S17a).

We expanded the reaction setup into a flow system to improve ethylene selectivity (Fig. 3f). Over a 240-minutes photothermal flow experiment, the catalyst consistently produced about 500 μmol·h^{-1} of ethylene, with selectivity rising to 97%, surpassing the batch reaction results.

2.4 Sunlight-driven non-oxidative ethane dehydrogenation.

To validate the feasibility of solar-powered thermal NOEDH, we developed a solar-concentrating setup (Fig. 4a) using a Fresnel lens for light focusing (Fig. 4b). Over four days, reactions were conducted with natural sunlight (Figs. 4c and 4d). The light intensity of one sun at various times and the actual temperature after focusing were precisely measured (Fig. S20), with corrections made for light loss passing through the Fresnel lens (Fig. S21). Under concentrated sunlight (about 463 fold natural intensity), 20 mL of ethane reached nearly 40% conversion in 10 minutes, with a maximum ethylene production rate of 1846 μmol h^{-1}, much higher than existing photocatalytic systems (Table. S1). The ethylene production rate depended on weather (light intensity) and solar concentration, as infrared and near-infrared radiation rapidly increased catalyst surface temperature and accelerated dehydrogenation and C–C bond cleavage. The solar-driven reaction produced more CH_4, reducing ethylene selectivity; carbon balance analysis suggests possible carbonaceous deposit formation. In summary, these results confirm the viability of TiN-based solar-driven NOEDH. The reaction rate matches that of commercial thermal catalysts, and both ethylene production rate and selectivity surpass previous photothermal studies.

In Press

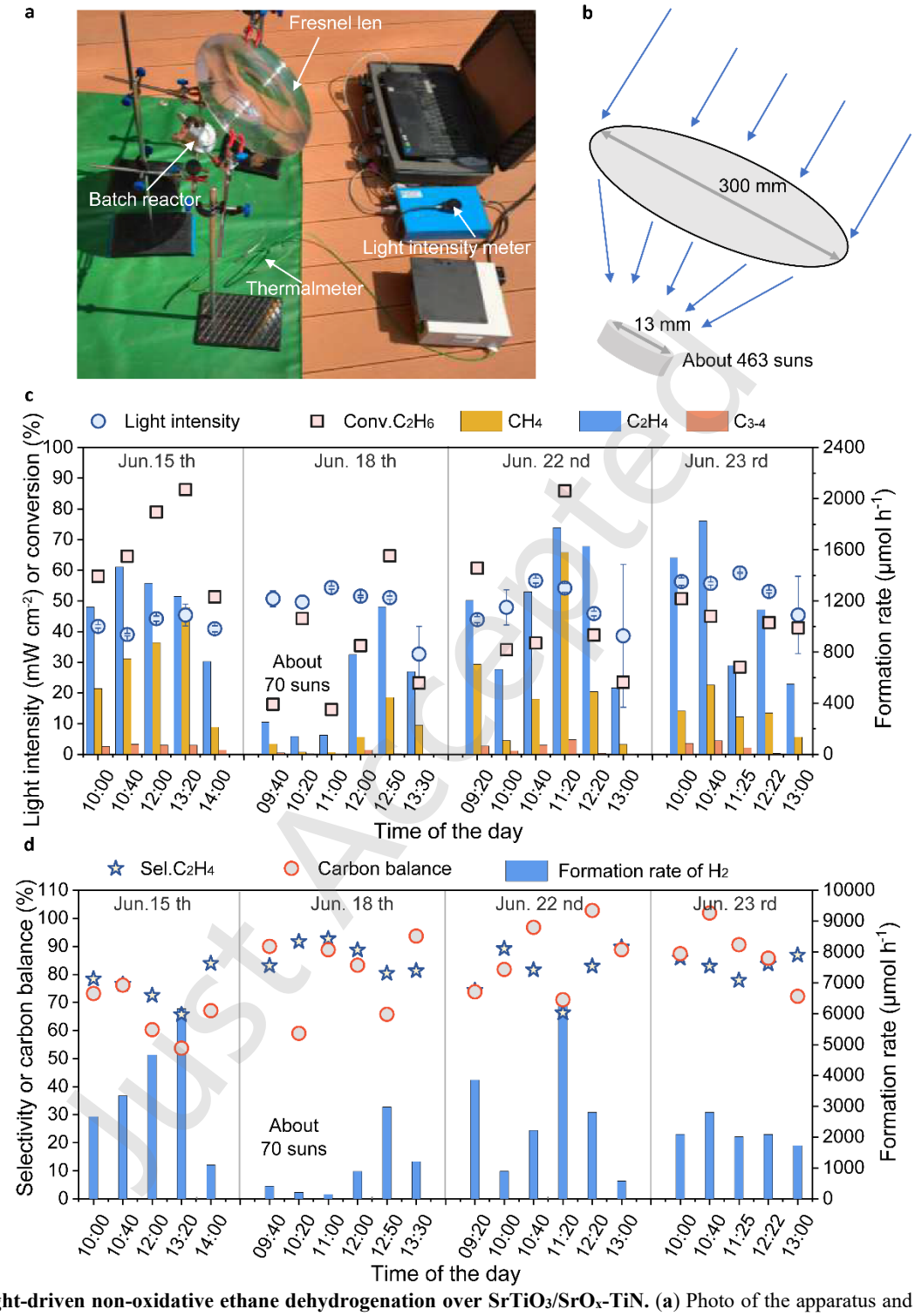


Fig. 4. Sunlight-driven non-oxidative ethane dehydrogenation over $SrTiO_3/SrO_x$-TiN. (**a**) Photo of the apparatus and (**b**) diagram of the reactor under irradiation by concentrated sunlight. (**c**) Light intensity, conversion, and formation rate of carbon products over 4 days of reaction. (**d**) Selectivity, carbon balance, and formation rate of H_2 over 4 days of reaction. Reaction conditions: 20 mL of C_2H_6 was injected into a 40 mL metallic reactor filled with 1 atm Ar, and 60 mg of catalyst was compressed into the metallic round groove and irradiated with concentrated solar light for 10 minutes, with an irradiation area of 706.5 cm^2 of natural solar light. Sunlight was concentrated into an area of 1.3 cm^2.

Just Accepted

3 Conclusion

In summary, the integration of experimental, spectroscopic, and theoretical approaches demonstrates the feasibility of sunlight-driven NOEDH. Using Sr as a case study, XRD and XAFS analyses showed structural changes after modification, confirming the formation of surface $SrTiO_3$. HRTEM and EDS mapping further verified the distribution of $SrTiO_3$ on the $SrTiO_3/SrO_x$-TiN surface. UV-Vis spectroscopy revealed improved visible-light absorption in the modified catalyst, while PL spectroscopy indicated increased electron-hole recombination at the interface, leading to an average temperature rise of 55 °C. COMSOL simulations showed that an interfacial electron-hole recombination heating power of 9×10^{-9} W caused the TiN temperature to increase by 51 °C. Collectively, these findings demonstrate a significant local temperature increase at the catalyst interface after surface modification, enhancing solar-to-thermal energy conversion efficiency.

Modifying the TiN catalyst with different metal ions considerably boosts activity in NOEDH, with Sr modification offering the most substantial increase, elevating activity by 11.7 times. Introducing Sr onto the surface aided in forming a $SrTiO_3$ perovskite phase, which enhanced interfacial electron-hole recombination. The catalytic reactivity improved with more exposed interfacial sites. Rigorous control experiments suggest that the $SrTiO_3$–TiN interface is likely the principal reaction site. Reaction results and cycling experiments confirmed that the modified $SrTiO_3/SrO_x$-TiN catalyst exhibits excellent activity and stability for ethane dehydrogenation. Furthermore, over four consecutive days under natural sunlight, we showed that the catalyst can reach a maximum ethylene production rate of 1846 μmol h^{-1} with 85.9% selectivity. The approach in this study, which creates numerous interfacial sites acting as effective electron-hole recombination centers, is crucial for advancing sophisticated heterogeneous solar photothermal catalytic systems.

4 Experimental section

4.1 Synthesis of $H_2Ti_4O_9$ nanotube (TNT).

$H_2Ti_4O_9$ nanotube (TNT) was synthesized using traditional hydrothermal methods with minor modifications. Typically, 90 mL of deionized water (18.2 MΩ cm^{-1}) was added to a 250 mL beaker. Under continuous stirring, 36 g of sodium hydroxide was slowly added. After the solution cooled, 3 g of P25 was added. After 24 h of vigorous stirring, the suspension was transferred to a 200 mL Teflon-lined autoclave and sealed in metallic cladding, then heated at 160 °C for 48 h. After completion, excess sodium hydroxide was removed by repeated washing with dilute nitric acid and finally thoroughly dried at 60 °C for at least 12 hours to obtain $H_2Ti_4O_9$ nanotubes.

4.2 Synthesis of MO_x/M-TiN nanocomposite.

A typical impregnation process was conducted to obtain the M^{n+}-modified oxide precursor (M-TNT) before nitridation. Specifically, 20 mL of deionized water (18.2 MΩ cm^{-1}) was added first to a 100 mL round-bottom flask. Then, 5 mL of the precursor solution (MCl_2) was added, followed by 500 mg of TNT. The flask was sealed and stirred for 24 h. The M^{n+}-modified oxide precursor (M-TNT) was obtained by rotary evaporation at 60 °C for 60 minutes. The final nitridation process involved taking 500 mg of the precursor, spreading it evenly, heating it to a specific temperature (T) at a rate of 10 °C $minute^{-1}$ in 250 mL $minute^{-1}$ NH_3, and maintaining this temperature for 3 h to obtain the desired nanocomposites. Sr-containing nanocomposites derived from different nitridation temperatures (T) were denoted as N-T.

Data availability

All data needed to support the conclusions in the paper are presented in the manuscript and/or the Electronic Supplementary Information. Additional data related to this paper may be requested from the corresponding author upon request.

Acknowledgements

This work was supported by the National Key R&D Program of China (2022YFA1504904), the CAS Project for Young Scientists in Basic Research (YSBR-140), the Department of Science & Technology of Liaoning province (2024021100-JH3/102), the Dalian Innovation Support Plan for High Level Talents (2022RG13), DICP (Grant: DICP I202326), the New Cornerstone Science Foundation (NCI202516). We also thank the instrumental support from Liaoning Key Laboratory of Biomass Conversion for Energy and Material. Specially, we thank the staff members of XAFS Beamline (https://cstr.cn/31124.02.SSRF.BL14W1) at Shanghai Synchrotron Radiation Facility (https://cstr.cn/31124.02.SSRF), for providing technical support and assistance in data collection and analysis. Finally, we thank Shanshan Chen from Nankai University, Nengchao Luo from Dalian Institute of Chemical Physics for providing useful discussions.

Author contributions

Zexuan Li, experimental design and analysis, manuscript preparation. Chenwei Ni, COMSOL simulation. Ping Jin, conceptualization, manuscript preparation and revision. Yu Wang, XAFS tests and analysis. Feng Wang, conceptualization, manuscript revision.

Competing interests

The authors have no competing interests to declare that are relevant to the content of this article.

Use of AI statement

"Schematic diagram of Scheme 1 was optimized by means of ByteDance Seed 4.0 large model"

Supplementary Information The online version contains supplementary material available at https://doi.org/10.26599/CF.2026.9200093

© The author(s) 2026. Published by Tsinghua University Press.

Just Accepted

References

[1] Gong, J.; Li, C.; Wasielewski, M. R. Advances in solar energy conversion. *Chemical Society Reviews* **2019**, *48* (7), 1862-1864.

[2] Sun, X.; Jiang, S.; Huang, H.; Li, H.; Jia, B.; Ma, T. Solar Energy Catalysis. *Angewandte Chemie International Edition* **2022**, *61* ,e202204880.

[3] Xing, C.; Mao, C.; Wang, S.; Zhou, Y.; Wu, L.; Zhang, D.; Kang, D.; Yang, D.; Gong, W.; Wei, W.; et al. Ambient solar thermal catalysis for polyolefin upcycling using copper encapsulated in silicon nanosheets and chloroaluminate ionic liquid. *Nature Catalysis* **2025**, *8* (6), 556-568.

[4] Liu, Y.; Zhong, Q.; Xu, P.; Huang, H.; Yang, F.; Cao, M.; He, L.; Zhang, Q.; Chen, J. Solar thermal catalysis for sustainable and efficient polyester upcycling. *Matter* **2022**, *5* (4), 1305-1317.

[5] Askes, S. H. C.; Garnett, E. C. Ultrafast Thermal Imprinting of Plasmonic Hotspots. *Advanced Materials* **2021**, *33* (49), 2105192.

[6] Jiang, D.; Wang, W.; Sun, S.; Zhang, L.; Zheng, Y. Equilibrating the plasmonic and catalytic roles of metallic nanostructures in photocatalytic oxidation over Au-modified CeO_2. *ACS Catalysis* **2014**, *5* (2), 613-621.

[7] Hu, X.; Wang, S.; Duan, R.; Li, A.; Li, J.; Feng, Z.; Zhai, M.; Wang, E.; Li, C. Structure regulation of TiO_2 with transition metal nitride units towards efficient solar energy harvesting. *Chemical Engineering Journal* **2025**, *519*, 165325.

[8] He, H.; Ren, Y.; Peng, R.; Zhang, H.; Zhu, Y. H.; Liu, X.; Zhou, J.; Duan, L.; Si, Y.; Liu, M.; et al. Nanoconfined photothermal catalysis: mechanisms, engineering strategies, and solar fuel synthesis. *Advanced Materials* **2026**, *38* (11), e23060.

[9] Cai, M.; Wu, Z.; Li, Z.; Wang, L.; Sun, W.; Tountas, A. A.; Li, C.; Wang, S.; Feng, K.; Xu, A.-B.; et al. Greenhouse-inspired supra-photothermal CO_2 catalysis. *Nature Energy* **2021**, *6* (8), 807-814.

[10] Meng, L.; Chen, Z.; Ma, Z.; He, S.; Hou, Y.; Li, H.-H.; Yuan, R.; Huang, X.-H.; Wang, X.; Wang, X.; et al. Gold plasmon-induced photocatalytic dehydrogenative coupling of methane to ethane on polar oxide surfaces. *Energy & Environmental Science* **2018**, *11* (2), 294-298.

[11] Sui, X.; Zhao, J.; Zhang, P.; Wang, Y.; Zheng, H.; Zeng, H.; Wang, P.; Jia, Y.; Wen, N.; Ding, Z.; et al. Photocatalytic non-oxidative dehydrogenation of ethane to ethene with near unit selectivity. *Nature Communications* **2025**, *16* (1), 9386.

[12] Zhang, P.; Li, J.; Huang, H.; Sui, X.; Zeng, H.; Lu, H.; Wang, Y.; Jia, Y.; Steele, J. A.; Ao, Y.; et al. Platinum single-atom nests boost solar-driven photocatalytic non-oxidative coupling of methane to ethane. *Journal of the American Chemical Society* **2024**, *146* (34), 24150-24157.

[13] Zou, Y.; Mao, C.; Xu, M.; Xing, C.; Wang, R.; Ozin, G. A.; Ling, L. Surface frustrated Lewis pairs in titanium nitride enable gas phase heterogeneous CO_2 photocatalysis. *Nature Communications* **2024**, *15* (1). 10604.

[14] Kaur, M.; Rej, S.; Navrátil, J.; Santiago, E. Y.; Otyepka, M.; Livraghi, S.; Mino, L.; Kment, Š.; Xu, Z.; Zhu, H.; et al. Near-infrared plasmonic activation of molecular oxygen for selective oxidation of biomass derivatives. *Nature Catalysis* **2025**, *8* (12), 1370-1381.

[15] Mao, C.; Wang, J.; Zou, Y.; Shi, Y.; Viasus, C. J.; Loh, J. Y. Y.; Xia, M.; Ji, S.; Li, M.; Shang, H.; et al. Photochemical acceleration of ammonia production by Pt_1-Pt_n-TiN reduction and N_2 activation. *Journal of the American Chemical Society* **2023**, *145* (24), 13134-13146.

[16] Afshar, M.; Schirato, A.; Mascaretti, L.; Hejazi, S. M. H.; Shahrezaei, M.; Della Valle, G.; Fornasiero, P.; Kment, Š.; Alabastri, A.; Naldoni, A. Nanoporous titanium oxynitride nanotube metamaterials with deep subwavelength heat dissipation for perfect solar absorption. *ACS Photonics* **2023**, *10* (9), 3291-3301.

[17] He, C.-Y.; Gao, X.-H.; Yu, D.-M.; Guo, H.-X.; Zhao, S.-S.; Liu, G. Highly enhanced thermal robustness and photothermal conversion efficiency of solar-selective absorbers enabled by high-entropy alloy nitride MoTaTiCrN nanofilms. *ACS Applied Materials & Interfaces* **2021**, *13* (14), 16987-16996.

[18] Wang, Q.-S.; Zhao, X.-B.; Dong, M.; Zheng, R.-B.; Gao, R.-T.; He, C.-Y.; Gao, X.-H. From metal nitrides to high-entropy nitrides: advances in spectrally selective absorber coatings. *EES Solar* **2025**, *1* (6), 898-926.

[19] Liu, H.-X.; Wang, W.-W.; Fu, X.-P.; Liu, J.-C.; Jia, C.-J. Direct cleavage of C=O double bond in CO_2 by the subnano MoO_x surface on Mo_2N. *Nature Communications* **2024**, *15* (1), 9126.

[20] Verma, S. S.; Sekhon, J. S. Influence of aspect ratio and surrounding medium on Localized Surface Plasmon Resonance (LSPR) of gold nanorod. *Journal of Optics* **2012**, *41* (2), 89-93.

[21] Li, Q.; Hu, Q.; Ding, Y.; Wu, H.; Yin, W.; Wen, Y.; Yang, R.; Wu, S.; Zhang, J. Interfacial oxide engineering of TiN antenna-reactor for durable photothermal dry reforming of methane. *Journal of the American Chemical Society* **2026**, *148* (22), 22827-22840.

[22] Rehman, A.; van de Kruijs, R. W. E.; van den Beld, W. T. E.; Sturm, J. M.; Ackermann, M. Work-function-dependent reduction of transition metal nitrides in hydrogen environments. *The Journal of Physical Chemistry Letters* **2024**, *15* (46), 11462-11467.

[23] Sun, Y.; Gong, K.; Li, T.; An, Y.; Sun, Q.; Lin, T.; Zhong, L. Ti3+-O Acid–base pairs for efficient solar-driven photothermal nonoxidative ethane dehydrogenation. *Journal of the American Chemical Society* **2026**, *148* (29): 31331–31342.

[24] Hu, Z.; Zhu, J.; Chen, R.; Wu, Y.; Zheng, K.; Liu, C.; Pan, Y.; Chen, J.; Sun, Y.; Xie, Y. High-rate and selective C_2H_6-to-C_2H_4 photodehydrogenation enabled by partially oxidized $Pd^{\delta+}$ species anchored on ZnO nanosheets under mild conditions. *Journal of the American Chemical Society* **2024**, *146* (24), 16490-16498.

[25] Liu, Y.; Xue, W.; Liu, X.; Wei, F.; Lin, X.; Lu, X. F.; Lin, W.; Hou, Y.; Zhang, G.; Wang, S. Ultrafine Pt nanoparticles on defective tungsten oxide for photocatalytic ethylene synthesis. *Small* **2024**, 20, 2402004.

[26] Song, R.; Zhao, G.; Restrepo-Flórez, J. M.; Viasus Pérez, C. J.; Chen, Z.; Ai, C.; Wang, A.; Jing, D.; Tountas, A. A.; Guo, J.; et al. Ethylene production via photocatalytic dehydrogenation of ethane using $LaMn_{1-x}Cu_xO_3$. *Nature Energy* **2024**, *9* (6), 750-760.

[27] Wang, Y.; Jiao, Y.; Ma, S.; Wei, Y.; Huang, W.; Fu, C. Size-engineered highly active and stable Pd/TiO_2 photocatalysts for selective oxidative dehydrogenation of ethane. *ACS Catalysis* **2025**, *15* (24), 20939-20946.

[28] Pan, L.; Ai, M.; Huang, C.; Yin, L.; Liu, X.; Zhang, R.; Wang, S.; Jiang, Z.; Zhang, X.; Zou, J.-J.; et al. Manipulating spin polarization of titanium dioxide for efficient photocatalysis. *Nature Communications* **2020**, *11* (1), 418.

Just Accepted